

# Thermal Gating in Lipid Membranes Using Thermoresponsive Cyclic Peptide–Polymer Conjugates

Maarten Danial,<sup>†</sup> Carmen M.-N. Tran,<sup>†</sup> Katrina A. Jolliffe,<sup>\*,‡</sup> and Sébastien Perrier<sup>\*,§,||</sup>

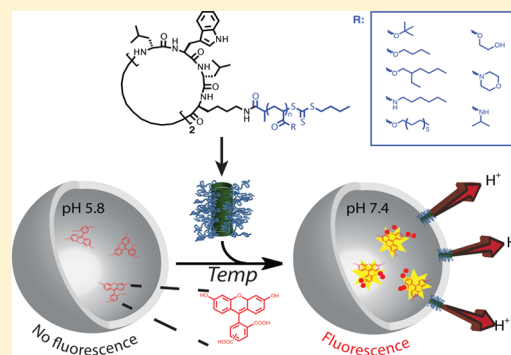
<sup>†</sup>Key Centre for Polymers & Colloids, <sup>‡</sup>School of Chemistry, The University of Sydney, Building F11, Sydney NSW 2006, Australia

<sup>§</sup>Department of Chemistry, The University of Warwick, Coventry, CV4 7AL, United Kingdom

<sup>||</sup>Faculty of Pharmacy and Pharmaceutical Sciences, Monash University, 381 Royal Parade, Parkville VIC 3052, Australia

## Supporting Information

**ABSTRACT:** The partition and self-assembly of a new generation of cyclic peptide–polymer conjugates into well-defined phospholipid trans-bilayer channels is presented. By varying the structural parameters of the cyclic peptide–polymer conjugates through the ligation of hydrophobic and hydrophilic polymers, both the structure of the artificial channels using large unilamellar vesicle assays and the structural parameters required for phospholipid bilayer partitioning are elucidated. In addition, temperature was used as an external stimulus for the modulation of transbilayer channel formation without requiring the redesign and synthesis of the cyclic peptide core. The thermoresponsive character of the cyclic peptide–polymer conjugates lays the foundation for on-demand control over phospholipid transmembrane transport, which could lead to viable alternatives to current transport systems that traditionally rely on endocytic pathways.



## INTRODUCTION

The biological membrane is one of the essential components of living cells.<sup>1</sup> Besides forming a barrier between cells and the external environment, it is an integral part of organelles and functions primarily to maintain homeostasis in the cell and within organelles. In order to preserve equilibrium across lipid bilayers in Nature, transmembrane protein channels form pathways that facilitate the regulation of ions, solutes, pH, and water and maintain optimal conditions for cellular and organelle environments. Despite the efficiency and selectivity of the natural transmembrane channels, both practical and large-scale production and the ability to tune their functionality remain significant challenges. The pursuit for cost-effective synthetic transmembrane channel alternatives for fundamental research and applied research has therefore attracted much attention in materials, chemical, and biological sciences in recent years.

A viable route to create artificial transmembrane channels is through molecular self-assembly.<sup>2–6</sup> Particularly over the past few years, evolution of molecular self-assembly from simple building blocks has emerged as a versatile process to construct functional, hierarchical transbilayer channel systems that are not readily achieved through conventional (bio)organic synthesis methods. Typical artificial channel architectures can be self-assembled from crown ethers,<sup>7,8</sup> cyclodextrins,<sup>9,10</sup> steroids,<sup>11</sup> oligoamides,<sup>12</sup> and aromatic macrocycles.<sup>6,13,14</sup> Recently, Chen et al. synthesized a pillar[5]arene that was derivatized with phenylalanine-containing peptide chains.<sup>14</sup> The ligation of peptide chains containing L-phenylalanine led to channels with chiral cavities favoring transport of a select number of D-

amino acids, thereby mimicking the natural function of amino acid transmembrane transporters.<sup>15</sup> Another type of hierarchical structure that can be self-assembled in lipid bilayers is based on cyclic peptide nanotubes.<sup>5,16–18</sup> These nanotubes are especially intriguing because they offer a functional utility and nanometer dimensions that are similar to transmembrane protein channels found in Nature.<sup>19,20</sup>

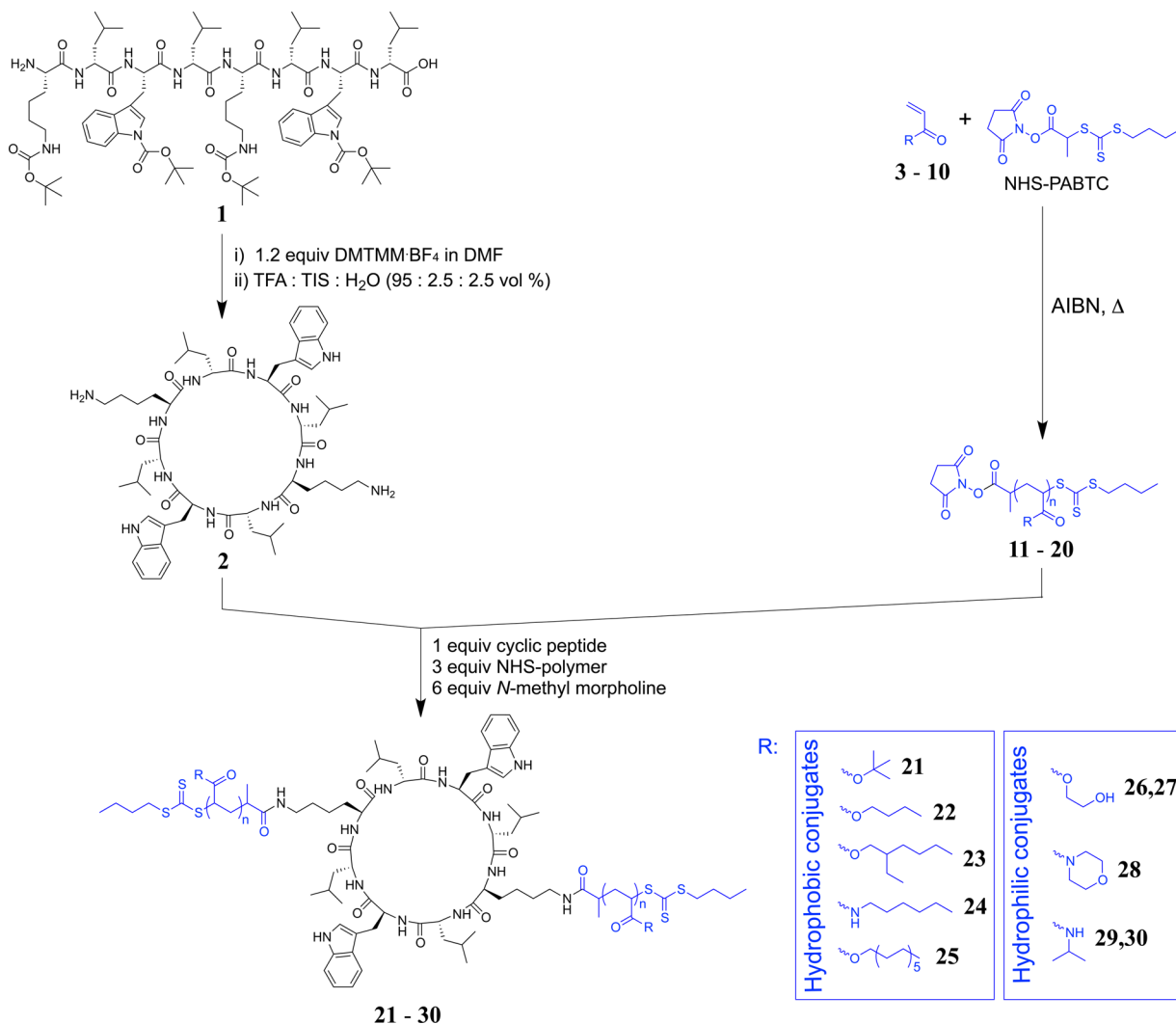
Although cyclic peptides have shown some potential as practical transbilayer transport channels for protons and ions,<sup>16,21,22</sup> glucose,<sup>23</sup> and glutamic acid,<sup>24</sup> more recent work has focused on cyclic peptides as antibacterials.<sup>25–27</sup> There are, however, many exciting possible applications for cyclic peptide channels, since they offer a direct transport route across the phospholipid bilayer, and also provide a viable alternative to endocytic transport, which results in the encapsulation of solutes that ultimately require endosomal/lysosomal escape to become active. However, modulation of phospholipid bilayer partitioning behavior and channel formation has been achieved to date through elegant yet complex syntheses, focusing on the modification of the cyclic peptide amino acid residue composition, for instance, with cyclic peptides containing a glycosyl serine<sup>27</sup> or  $\gamma$ -amino acids.<sup>17,28</sup> Construction of large libraries of different compounds is therefore time-consuming and synthetically challenging, thus limiting applications.

In this manuscript we demonstrate how phospholipid bilayer partitioning and channel formation can be achieved and finely tuned, without redesigning the cyclic peptide core. The types of

Received: March 13, 2014

Published: May 9, 2014

Scheme 1. Convergent Synthesis Approach for the Production of Cyclic Peptide–Polymer Conjugates



channels formed in the phospholipid bilayer are revealed using large unilamellar vesicles (LUVs) containing entrapped fluorescent dyes. Using a series of hydrophobic and hydrophilic polymers ligated to the cyclic peptide moiety allowed for the elucidation of structure–channel formation relationships. With the knowledge gained, we demonstrate the formation of unique temperature responsive transbilayer channels using cyclic peptide–poly(*N*-isopropylacrylamide) conjugates. As a consequence we envision that the research presented here will open up new avenues for the creation of direct, nonendocytic transport links across biological phospholipid membranes without causing significant membrane distortion.

## RESULTS AND DISCUSSION

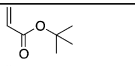
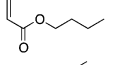
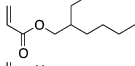
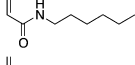
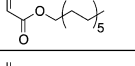
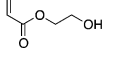
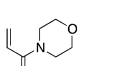
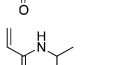
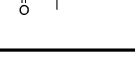
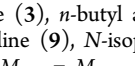
**Design and Synthesis Rationale.** The cyclic peptide–polymer nanotubes described herein are based on cyclic peptides containing eight alternating  $\alpha$ -D,L-amino acid residues.<sup>31</sup> The alternating  $\alpha$ -D,L-amino acid configuration leads to contiguous hydrogen bonding along the cyclic peptide stacks since the amide bonds are projected perpendicular to the plane of the cyclic peptide.<sup>29,30</sup> In addition, the amino acid side chains are projected out of the cyclic peptide plane in pseudoequatorial positions, which allows for synthetic modification without causing interference with the nanotubular self-

assembly. An octameric cyclic peptide was chosen since thermodynamic studies on the *N*-alkylated cyclic peptide analogues indicated higher association constants for these than for cyclic peptides consisting of 4, 6, 10, or 12 amino acids.<sup>20</sup>

Modification of cyclic peptides with macromolecules<sup>31–35</sup> has shown that functionality and pseudocontrol over nanotube length can be imparted onto the cyclic peptide–polymer nanotubes without having to alter the amino acid constitution. There are two strategies that can be employed to create cyclic peptide–polymer conjugates. The divergent approach, by which the polymer chains are grafted from the cyclic peptide, offers a single synthesis step to produce cyclic peptide–polymer conjugates but does not permit easy access to the controlled molecular weight, dispersity ( $M_w/M_n$ ), and grafting density of the polymer chains attached to the cyclic peptide. Conversely, the convergent approach, by which pre-made polymer chains are attached to the cyclic peptide, is a more versatile methodology since cyclic peptide and polymer can be individually characterized prior to conjugation and self-assembly.

Scheme 1 depicts the convergent approach that was employed to create a library of cyclic peptide–polymer conjugates. This library was designed to establish which polymer structures had the propensity to partition into

Table 1. Polymerization Conditions and Molecular Weight Analysis of the Polymers Synthesized

Polymer	Monomer, M <sup>a</sup>	[M] / [CTA]	Conv., x <sup>b</sup> (%)	M <sub>n,th</sub> <sup>c</sup> (g·mol <sup>-1</sup> )	DP <sub>n,th</sub> <sup>d</sup> (-)	M <sub>n,SEC</sub> <sup>e</sup> (g·mol <sup>-1</sup> )	M <sub>w</sub> /M <sub>n</sub> <sup>e</sup> (-)	M <sub>n,NMR</sub> <sup>f</sup> (g·mol <sup>-1</sup> )	DP <sub>n,NMR</sub> <sup>f</sup> (-)		
Hydrophobic polymers	<b>11</b>		3	50	68	4690	34	3900	1.12	4000	31
	<b>12</b>		4	50	90	6100	45	5000	1.18	5400	42
	<b>13</b>		5	50	84	8070	42	7000 <sup>g</sup>	1.16 <sup>g</sup>	7200	38
	<b>14</b>		6	100	61	9800	61	9100	1.18	9000	58
	<b>15</b>		7	50	64	7130	32	6000 <sup>g</sup>	1.17 <sup>g</sup>	6100	29
Hydrophilic polymers	<b>16</b>		8	40	88	4420	35	4100	1.23	3600	31
	<b>17</b>		9	120	83	11890	100	14400	1.24	10900	94
	<b>18</b>		10	60	67	6010	40	3200	1.18	5200	37
	<b>19</b>		10	50	90	5420	45	5900	1.14	5400	48
	<b>20</b>		10	100	88	10290	88	11900	1.18	10700	95

<sup>a</sup>*t*-Butyl acrylate (3), *n*-butyl acrylate (4), 2-ethylhexyl acrylate (5), *N*-hexyl acrylamide (6), lauryl acrylate (7), 2-hydroxyethyl acrylate (8), 4-acryloylmorpholine (9), *N*-isopropylacrylamide (10). <sup>b</sup>Conversion (*x*) determined by <sup>1</sup>H NMR. <sup>c</sup>Theoretical number-average molecular weight obtained using  $M_{n,th} = M_{CTA} + [M]/[CTA] \cdot M_{Monomer} \cdot x$ . <sup>d</sup>Degree of polymerization obtained using  $DP = (M_{n,th} - M_{CTA})/M_{Monomer}$ . <sup>e</sup>Number-average molecular weight and dispersity from DMF SEC relative to polystyrene standards. <sup>f</sup>Number-average molecular weight and degree of polymerization determined using the  $\alpha$ -chain end succinimidyl group. <sup>g</sup>Number-average molecular weight and dispersity from THF SEC relative to polystyrene standards.

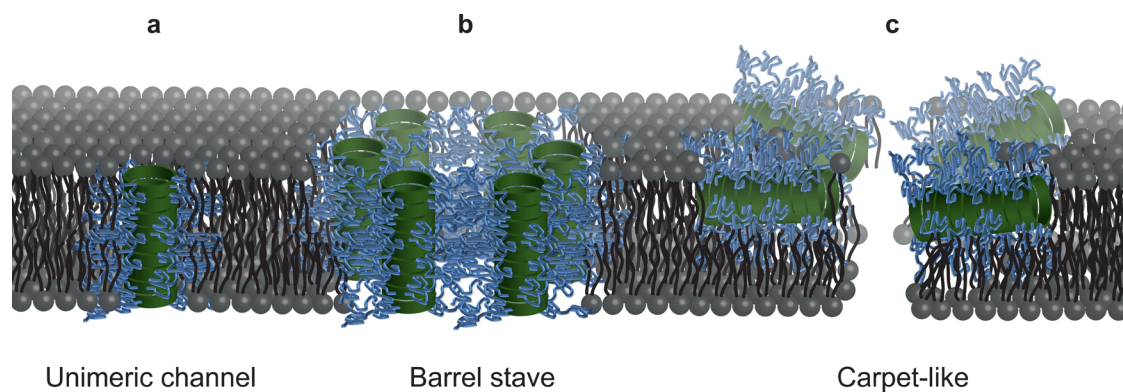


**Figure 1.** Cyclic peptide–polymer conjugates can exhibit different modes of phospholipid bilayer disruption in the form of (a) unimeric channels or (b) barrel staves or (c) as a carpet-like bilayer disruption.

phospholipid bilayers. The envisioned conjugates consisted of a series of hydrophobic and hydrophilic polymers (11–20) ligated to a central cyclic peptide moiety (2). The polymers were synthesized via reversible addition–fragmentation chain transfer (RAFT) polymerization<sup>36–38</sup> using an *N*-hydroxysuccinimidyl 2-propionic acid butyl trithiocarbonate (NHS-PABTC) chain transfer agent.<sup>39</sup> As Table 1 reveals, all polymers synthesized had low dispersity values and the number-average molecular weight determined from <sup>1</sup>H NMR was in good agreement with values obtained by size exclusion chromatography (SEC). Furthermore, <sup>1</sup>H NMR spectra demonstrated that the protons corresponding to the succinimidyl group remained after polymer purification, which provides evidence that the active ester remained intact. More notably, the peaks in

the <sup>1</sup>H NMR spectrum corresponding to the succinimidyl protons of poly(*t*-butyl acrylate) (11) and poly(*n*-butyl acrylate) (12) remained after precipitation of these polymers was performed in a mixture of water and methanol, suggesting strong resilience of the active ester in the presence of weak (hydroxyl) nucleophiles (see Supporting Information Figure S1 and S2, respectively). Further support for the resilience of the  $\alpha$ -chain end succinimidyl active ester in the presence of multiple hydroxyl groups was evident from <sup>1</sup>H NMR analysis of purified poly(2-hydroxyethyl acrylate)s 16 and 17 (see Figure S3).

The protected linear peptide precursor (1) was synthesized by Fmoc-solid phase peptide synthesis (Figures S4 and S5). After cleavage from the chlorotrityl resin, the linear peptide was

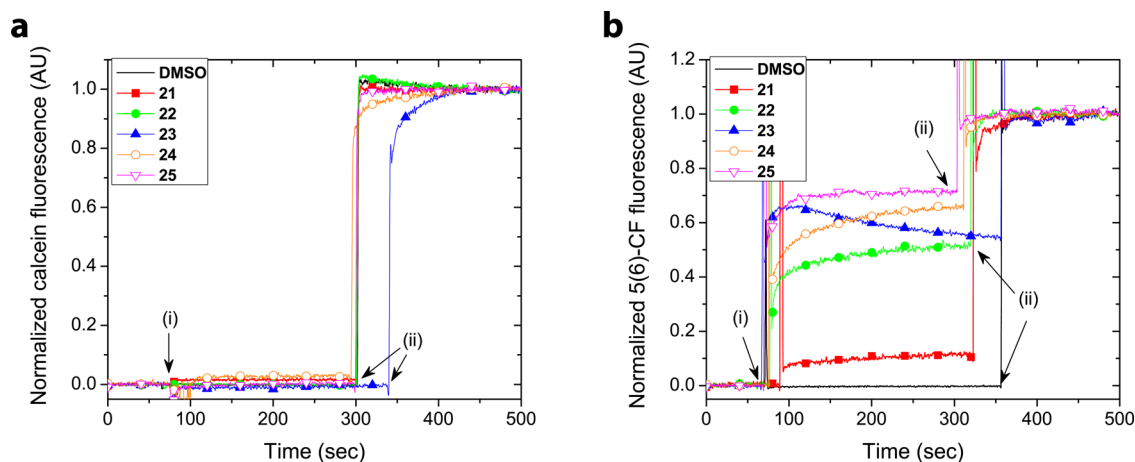


**Figure 2.** Bilayer activity of 19.6  $\mu\text{M}$  hydrophobic conjugates using (a) calcein-entrapped LUVs made from egg yolk phosphatidylcholine demonstrating the absence of barrel staves and carpet-like bilayer disruption and (b) 5(6)-carboxyfluorescein-entrapped LUVs made from egg yolk phosphatidylcholine demonstrating the presence of unimeric channels per LUV. The sample (40  $\mu\text{L}$  of 1 mM stock solution) is added to the solution containing LUVs (2 mL) at (i)  $\sim 70$  s followed by (ii) Triton X-100 (40  $\mu\text{L}$  of 1% w/v) at  $\sim 300$  s.

cyclized. The structures of the Boc-protected and Boc-deprotected cyclic peptides (**1a** and **2**, respectively) were confirmed using  $^1\text{H}$  NMR and distortionless enhancement by polarization transfer-edited heteronuclear single quantum coherence (DEPT-ed-HSQC) NMR spectroscopy (Figures S6–S9). Ultimately, a library of conjugates (**21–30**) was generated through the ligation of succinimidyl-ester  $\alpha$ -terminated polymers with cyclic peptide **2**, which contains two lysine handles, in the presence of *N*-methyl morpholine. Purification of the conjugates was achieved using preparative size exclusion chromatography to remove the excess succinimidyl-ester terminated polymer required for the conjugation reaction (see Figures S10 and S11).

#### Formation and Elucidation of Transbilayer Channels.

As depicted in Figure 1, the different types of transbilayer channels formed by the cyclic peptide–polymer conjugates may consist of (i) unimeric channels, (ii) barrel staves oligomers, or (iii) carpet-like bilayer disruption. As multiple modes of bilayer channel formation are feasible, fluorescence spectroscopy was used to assess the actual type of channel formed by the different cyclic peptide–polymer conjugates presented in this report. To this end, a series of assays that follow the changes in fluorescence intensity of fluorescent dyes upon bilayer pore formation was utilized.<sup>40</sup> To establish the size of the pore, calcein-entrapped and 5(6)-carboxyfluorescein-entrapped LUV assays were performed. The calcein-entrapped LUVs were used to determine whether the conjugates form a barrel stave or disrupt the phospholipid bilayer via a carpet-like interaction (Figure 1b and c). Calcein dye leakage through the barrel stave or carpet-like disrupted bilayer causes a decrease in self-quenching and leads to an increase in fluorescence emission (Figure S12). If no calcein dye leakage from the LUVs occurred, thereby discounting the formation of barrel staves or carpet-like bilayer disruption, a 5(6)-carboxyfluorescein-entrapped LUVs assay was used to establish the presence of unimeric channels (Figure 1a). The pH-responsive fluorescent dye 5(6)-carboxyfluorescein has a strong emission at neutral pH but a weak emission in acidic pH.<sup>41</sup> The formation of unimeric channels upon addition of the conjugates can be tested by establishing a pH gradient across the phospholipid bilayer, whereby the internal LUV environment consists of phosphate buffer at pH 5.8 and the external environment

consists of a phosphate buffer at pH 7.4. Formation of unimeric channels in the phospholipid bilayer results in the collapse of the pH gradient through the efflux of protons and causes the 5(6)-carboxyfluorescein emission intensity to increase (Figure S12).<sup>42</sup>

In order to assess the type of channels formed as depicted in Figure 1, LUVs consisting of egg yolk phosphatidylcholine were produced via the extrusion of the lipid-containing solution through a 100 nm pore size polycarbonate membrane. The fluorescence of these dye-entrapped LUVs was monitored and included a  $\sim 70$  s baseline after which a sample of conjugate was added followed by the addition of Triton X-100 at  $\sim 300$  s, which causes lysis of the phospholipid LUVs and enables the normalization of data relative to the maximum fluorescence emission. The samples were prepared as stock solutions in dimethyl sulfoxide (DMSO) from which an aliquot was added to the cuvette containing the LUVs in phosphate buffered aqueous solution yielding a final concentration of 19.6  $\mu\text{M}$  in  $< 2\%$  DMSO. As shown in Figure 2a, addition of hydrophobic conjugates **21–25** to the LUVs caused less than 1% calcein dye leakage consistent with the absence of barrel staves or carpet-like bilayer disruption. Furthermore, no adverse fluorescence increase consistent with vesicle lysis was observed, suggesting that the conjugates do not induce nonspecific phospholipid interactions. However, assessment of unimeric channel formation using 5(6)-carboxyfluorescein-entrapped LUVs revealed that the pH gradient across the phospholipid bilayer subsided in the presence of 19.6  $\mu\text{M}$  of the hydrophobic conjugates **21–25** (Figure 2b). Furthermore, the unconjugated polymers (**11–20**) do not cause calcein dye leakage and do not cause significant collapse of the pH gradient across the phospholipid bilayer demonstrating that the cyclic peptide moiety is required for transbilayer channel transport of protons (Figure S13).

The phospholipid bilayer partitioning activity seems to follow a trend that depends on the lipophilicity. Conjugate **25** which has a poly(lauryl acrylate) shell exhibits a 71% change in 5(6)-carboxyfluorescein emission, while conjugate **21**, which has a poly(*t*-butyl acrylate) shell, exhibits only a marginal change in 5(6)-carboxyfluorescein emission (10%). As shown in Table 2, comparison of the logP values (a measure of the lipophilicity of the conjugates) based on the monomer structure obtained by

**Table 2. Structure–Phospholipid Bilayer Partitioning Activity of the Hydrophilic and Hydrophobic Cyclic Peptide–Polymer Conjugates**

conjugate	polymer precursor <sup>a</sup>	XlogP3 <sup>b</sup> (-)	$\Delta f^c$ (%)
Hydrophobic Conjugates			
21	poly( <i>t</i> -butyl acrylate) <sub>31</sub>	11	1.69
22	poly( <i>n</i> -butyl acrylate) <sub>42</sub>	12	2.36
23	poly(2-ethylhexyl acrylate) <sub>38</sub>	13	3.83
24	poly( <i>N</i> -hexyl acrylamide) <sub>58</sub>	14	2.47
25	poly(lauryl acrylate) <sub>29</sub>	15	6.17
Hydrophilic Conjugates			
26	poly(2-hydroxyethyl acrylate) <sub>31</sub>	16	-0.21
27	poly(2-hydroxyethyl acrylate) <sub>94</sub>	17	-0.21
28	poly(4-acryloylmorpholine) <sub>37</sub>	18	-0.06
29	poly( <i>N</i> -isopropylacrylamide) <sub>48</sub>	19	0.93
30	poly( <i>N</i> -isopropylacrylamide) <sub>95</sub>	20	0.93

<sup>a</sup>Polymer ligated to the cyclic peptide using the  $\alpha$ -chain end NHS chemistry. The subscripts denote the degree of polymerization determined using the  $\alpha$ -chain end succinimidyl group. <sup>b</sup>logP calculation according to a training set of 8199 compounds according to Cheng et al.<sup>43</sup> To aid simplicity of the computation, the XlogP3 values were calculated using chemical structures of the monomers and therefore do not take into account the degree of polymerization of the polymers. <sup>c</sup>Percentage change in 5(6)-carboxyfluorescein emission at 280 s relative to LUV lysis at 22 °C.

the XlogP3 computational algorithm<sup>43,44</sup> revealed a trend between lipophilicity and the percentage change in 5(6)-carboxyfluorescein emission. Expressing the trend observed for the cyclic peptides modified with hydrophobic polymers in terms of percentage change in 5(6)-carboxyfluorescein emission ( $\Delta f$ ) revealed the order  $25 > 24 > 23 > 22 \gg 21$ . In comparison, the calculated logP values followed a similar trend  $25 > 23 > 24 \approx 22 > 21$ , which can be attributed to differences in lipophilicity between the monomer and polymers as well as the slight differences in degree of polymerization of the polymers attached to the cyclic peptide. Closer inspection of the LUV sample with conjugate 23 revealed that precipitation was taking place and led to a reduction in fluorescence after a rapid initial increase (Figure 2). Thus, a lower than expected change in fluorescence observed for

conjugate 23 might be due to precipitation, a process that the logP calculation does not take in to account. Branched structures have been known to exhibit a higher partitioning in phospholipid bilayers than their nonbranched counterparts<sup>45</sup> and also exhibit limited solubility in aqueous solutions,<sup>46</sup> which may explain why the observed changes in fluorescence do not follow exactly the same trend as the logP values (conjugate 23 contains a branched polymer side chain, whereas 24 and 25 have nonbranched polymer side chains). Previous studies have shown that modifying tryptophan to glutamine residues,<sup>16</sup> as well as replacing homotryptophan with homoleucine residues<sup>18</sup> in cyclic peptides, eradicates phospholipid bilayer partitioning, although an elaborate study on the effect on bilayer partitioning of cyclic peptides that vary in the degree of lipophilicity is still lacking. Given that in the present system, the cyclic peptide core was not altered, the structure of the polymeric chains clearly has a significant effect on the membrane partitioning of these conjugates.

Having established that cyclic peptide–polymer conjugates consisting of a hydrophobic shell partition into phospholipid bilayers and form well-defined single channels, the role of lipophilicity was compared to cyclic peptide–polymer conjugates consisting of a hydrophilic shell. A series of conjugates were prepared through the ligation of hydrophilic polymers poly(2-hydroxyethyl acrylate)s 16 and 17, poly(4-acryloylmorpholine) 18, and poly(*N*-isopropylacrylamide) 19 and 20 to the cyclic peptide (Scheme 1). The solubility of the constituent polymers of conjugates 26–30 in a range of organic solvents including aprotic solvents (e.g., 16–20 in DMF and DMSO) and nonpolar solvents (e.g., 18–20 in toluene and chloroform) suggested compatibility with phospholipid bilayers. Thus, despite these conjugates being classified as “hydrophilic”, minimal channel formation in LUV bilayers was expected. As shown in Figure 3a, the hydrophilic cyclic peptide–polymer conjugates did not form barrel staves or cause bilayer disruption and is consistent with the observations made with the hydrophobic conjugates 21–25.

Despite the apparent hydrophilicity of the polymer chains of conjugates 26–30, unimeric channel formation still occurs (Figure 3b), albeit to a much lesser extent than for the hydrophobic conjugates 21–25. Presumably, the nonhydro-

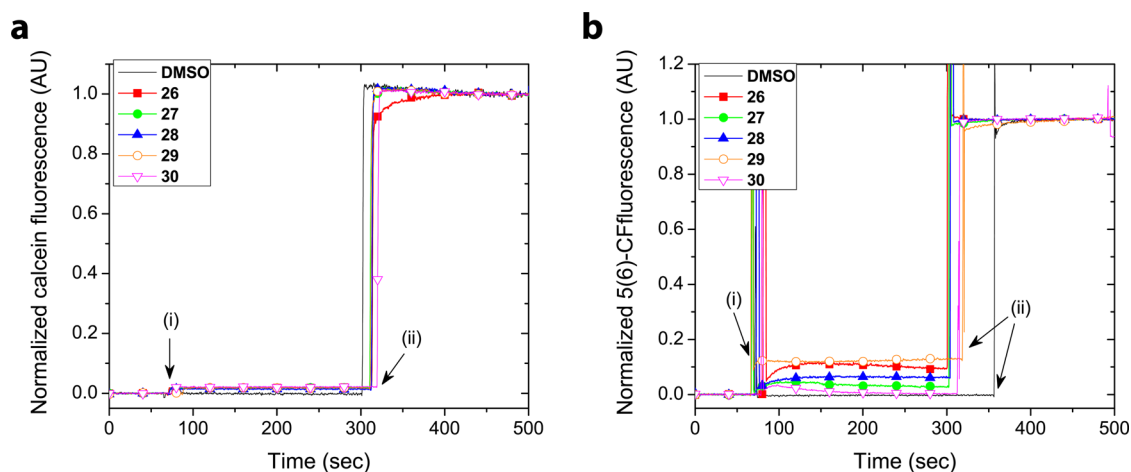


**Figure 3.** Bilayer activity of 19.6  $\mu$ M hydrophilic conjugates using (a) calcein-entrapped LUVs made from egg yolk phosphatidylcholine demonstrating the absence of barrel staves and carpet-like bilayer disruption and (b) 5(6)-carboxyfluorescein-entrapped LUVs made from egg yolk phosphatidylcholine demonstrating the presence of a small number of unimeric channels per LUV. The sample (40  $\mu$ L of 1 mM stock) is added to the solution containing LUVs (2 mL) at (i)  $\sim$ 70 s followed by (ii) Triton X-100 (40  $\mu$ L of 1% w/v) at  $\sim$ 300 s.

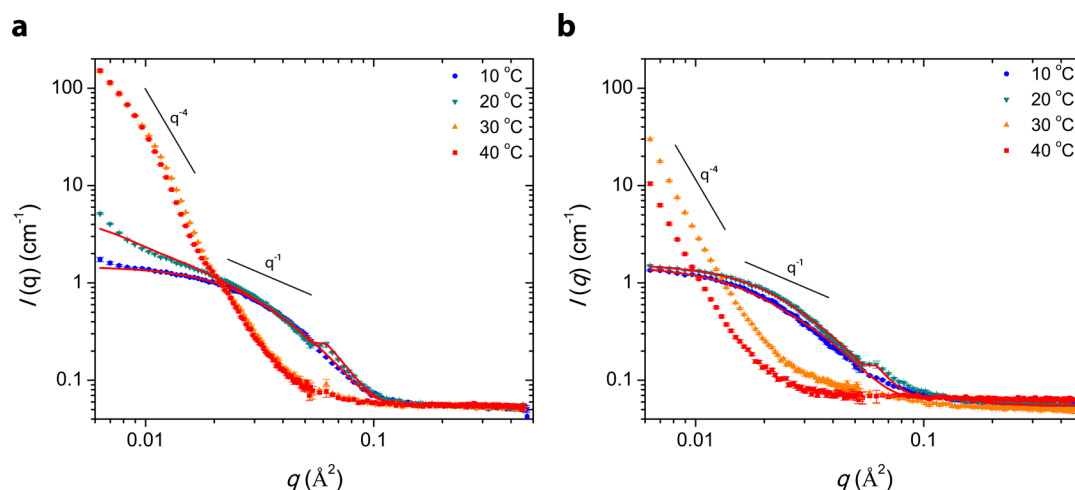


**Figure 4.** Temperature dependence on self-assembly of cyclic peptide–poly(*N*-isopropylacrylamide) conjugates in D<sub>2</sub>O:DMSO-*d*<sub>6</sub> (9:1 v/v). (a) Small angle neutron scattering of cyclic peptide–poly(NIPAAm)<sub>48</sub> conjugate 29. (b) Small angle neutron scattering of cyclic peptide–poly(NIPAAm)<sub>95</sub> conjugate 30. The scattering profiles for 10 and 20 °C are fit using a core–shell cylinder model. Scattering profiles of 30 and 40 °C cannot be fit using a cylinder-type model.

philic parts of the polymer, e.g., the aliphatic carbons, still induce partitioning into a lipid bilayer. In addition, the molecular weight of the polymers ligated to the cyclic peptide also has a profound effect on unimeric channel formation. As Table 2 reveals, cyclic peptide–poly(2-hydroxyethyl acrylate) conjugate 26 yielded a higher change in fluorescence emission than conjugate 27. This phospholipid partitioning effect corroborates well with the limited solubility of small chain poly(2-hydroxyethyl acrylate) conjugates in water reported elsewhere<sup>47</sup> and thus implies that conjugates with short chain “hydrophilic” polymers ligated have a greater degree of lipophilicity than their long chain polymer conjugate counterparts. Nevertheless, the low degree of lipophilicity of the hydrophilic conjugates results in far less effective single channel formation in phospholipid bilayers than that observed for hydrophobic conjugates. Furthermore, the hydrophilic polymers 16–20 did not result in calcein dye release or lead to 5(6)-carboxyfluorescein fluorescence emission and thus did not exhibit any pore formation in phospholipid bilayers (Figure S14). These results suggest that the cyclic peptide is an essential component of unimeric channel formation providing a direct transport route for the diffusion of protons from the LUV interior into the external medium.

Attempts to characterize the assembly of the cyclic peptide–polymer conjugates in intact LUV bilayers using Fourier transform infrared spectroscopy did not yield fruitful results due to two main issues. First, the separation of the LUVs containing unimeric channels from the unpartitioned cyclic peptide–polymer nanotubes using a Sephadex column proved challenging as the LUVs and cyclic peptide–polymer nanotubes coelute. Second, the characterization after subtraction of LUVs in the absence of cyclic peptide–polymer conjugates was inconclusive as the carbonyl stretch frequency derived from the acrylate/acrylamide polymer side chain as well as O–H bend frequency overlapped with the cyclic peptide amide I stretch that is characteristic for  $\beta$ -sheet (typically observed at  $\sim 1630$  cm<sup>-1</sup>). In addition, the N–H stretch (typically observed at  $\sim 3270$  cm<sup>-1</sup>) with cyclic peptide<sup>16</sup> and cyclic peptide–polymer nanotubes<sup>39,48</sup> overlaps with the broad O–H signal due to the presence of water, making it impossible to determine the

presence of hydrogen bonding as well as the distance between the cyclic peptide stacks.

**Thermoresponsive Channel Formation.** Artificial transmembrane channels could offer a route that circumvents the conventional modes of ion or molecule transport by forming a direct path and thus leading to minimal disruption to the integrity of phospholipid bilayers. Application of these artificial transmembrane channels on cells could prove beneficial over other methods for enabling compounds to pass the cell surface membrane such as electroporation,<sup>49</sup> sonoporation,<sup>50</sup> or magnetofection,<sup>51</sup> or via carrier nanoparticles.<sup>52</sup> Furthermore, Singhal et al., demonstrated that subcellular environments probed with a multiwalled carbon nanotube mounted on a glass pipet displaced less cellular material and induced less stress than conventional glass pipettes leading to a lower rate of cell fatality.<sup>53</sup> Besides hypothetically causing less cellular stress, the artificial transmembrane channels presented here could find potential as drug delivery transporters since endocytosis of the drug is avoided and lysosomal/endosomal escape mechanisms are not required to induce drug efficacy.<sup>52</sup> While cyclic peptide–polymer conjugates consisting of hydrophobic polymers partition in phospholipid bilayers and form well-defined channels (vide supra), the system lacks control as well as specificity. A temperature-induced system such as “thermal gating”<sup>54</sup> was envisioned which permits localized, on-demand phospholipid partitioning and channel formation triggered by tuning of the temperature. Besides forming an interesting tool to study and modulate ion flux across bilayers, these stimuli-responsive materials could spark interest in controlled drug delivery via hyperthermia.<sup>55</sup>

Conjugates consisting of a PNIPAAm shell were used to create the temperature-induced transbilayer channels. PNIPAAm exhibits a lower critical solution temperature (LCST) at  $\sim 32$  °C at which the water-soluble polymer becomes hydrophobic (or lipophilic). Despite the lower solubility of conjugate 29, which consisted of a PNIPAAm<sub>48</sub> shell, an LCST transition was evident at 25 °C (Figure S15). Conversely, conjugate 30, which consisted of a PNIPAAm<sub>95</sub> shell was fully soluble at room temperature and exhibited an LCST at 28 °C (Figure S15). Using small angle neutron scattering (SANS), the apparent difference in solubility in aqueous buffer was ascribed

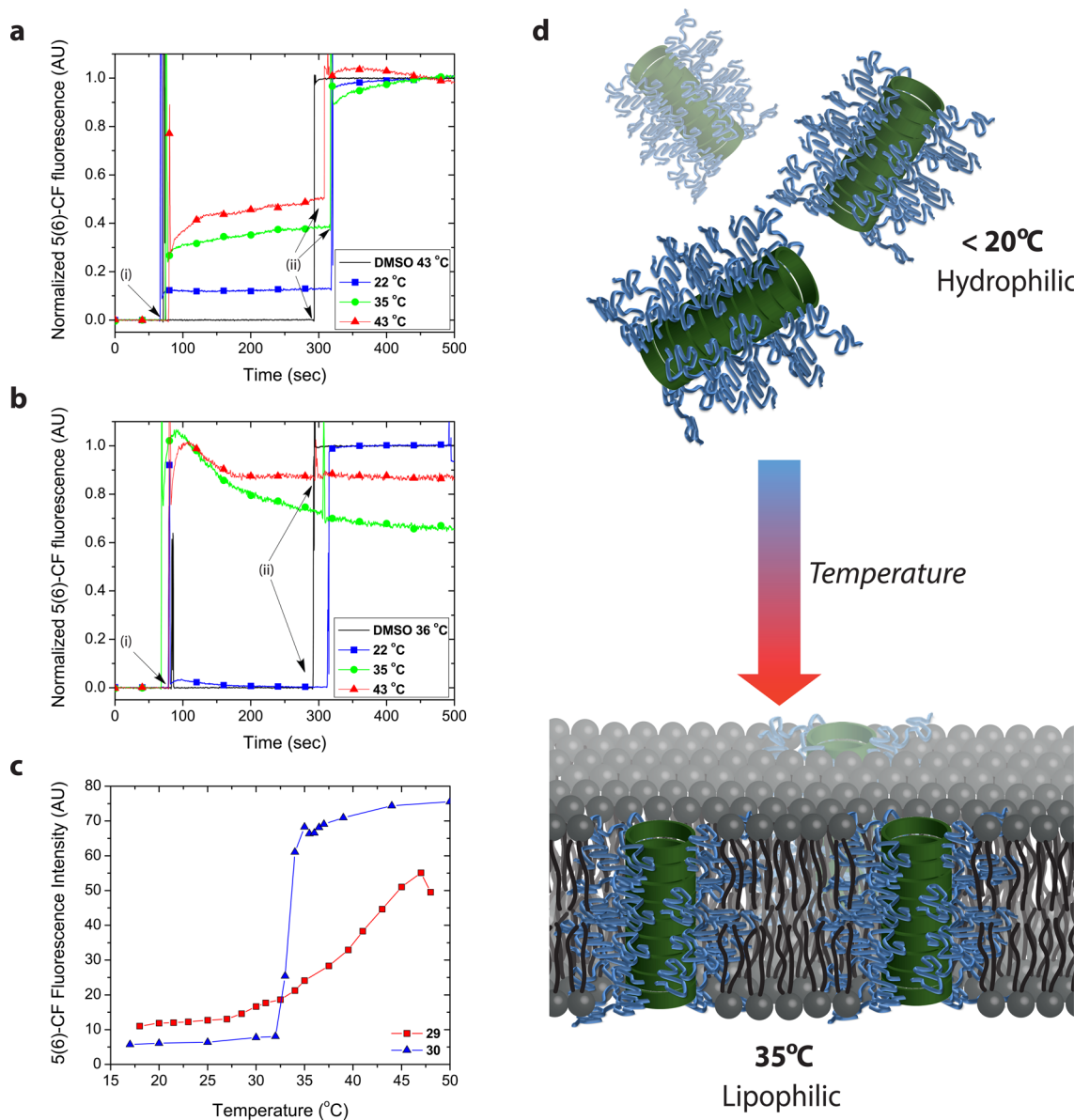


**Figure 5.** Effect of temperature on fluorescence of 5(6)-carboxyfluorescein-entrapped in LUVs made from egg yolk phosphatidylcholine in the presence of (a)  $19.6 \mu\text{M}$  cyclic peptide–poly(NIPAAm)<sub>48</sub> conjugate **29** and (b)  $19.6 \mu\text{M}$  cyclic peptide–poly(NIPAAm)<sub>95</sub> conjugate **30**. The sample is added at (i)  $\sim 70$  s followed by (ii) Triton X-100 at  $\sim 300$  s. (c) Proton efflux from LUVs incubated with  $19.6 \mu\text{M}$  conjugates as a function of temperature. (d) Illustration of well-defined unimeric channels formed upon heating the solution up to an intermediate temperature of  $35 \text{ }^\circ\text{C}$  in the presence of LUVs.

to a thicker PNIPAAm shell of conjugate **30** compared to conjugate **29**, which shields the solvent from interactions with the cyclic peptide core (Table S1). Similar to observations made by Chapman et al.,<sup>48</sup> the longer, more flexible polymers on conjugate **30** provide better shielding of the cyclic peptide core from the competitive aqueous solvent than smaller, rigid polymers on conjugate **29**. As shown in Figure 4, the SANS scattering profiles of the PNIPAAm conjugates **29** and **30** fit well to a core–shell cylinder model at temperatures below the LCST with nanotube lengths between 30 and 70 nm. An abrupt change in scattering profiles obtained at  $30 \text{ }^\circ\text{C}$  indicates that the nanotube structures are not retained at and above the LCST. The  $q^{-4}$  dependency at low scattering vectors observed at and above the LCST is indicative of precipitation consistent with typical behavior of hydrophobic species in aqueous solutions. In addition, the abrupt change in structure which

demonstrates that the nanotubes disassemble at the LCST is consistent with earlier work performed with thermoresponsive cyclic peptide–poly(2-ethyl-2-oxazoline) conjugates in which large spherical microparticles and precipitates were obtained above the LCST.<sup>56</sup>

Besides becoming lipophilic above the LCST, we anticipated that the PNIPAAm conjugates would retain the nanotubular structures due to favorable van der Waals interactions with phospholipid chains present in the bilayer of the LUVs. Incubation of the conjugates with 5(6)-carboxyfluorescein-entrapped LUVs made from egg yolk phosphatidylcholine at room temperature ( $22 \text{ }^\circ\text{C}$ ) resulted in a change in fluorescence emission that was consistent with other hydrophilic conjugates shown in Figure 3 (vide supra). As was observed for conjugates **26** and **27**, the shorter polymer chains of **29** resulted in a higher change in fluorescence emission than the cyclic peptide–

PNIPAAm<sub>95</sub> conjugate **30** upon incubation with 5(6)-carboxyfluorescein-entrapped LUVs. As shown in Figure 5, raising the temperature to 35 °C gave a ~34% and ~70% rise in fluorescence emission, respectively (Table 3), as conjugates **29**

**Table 3. Summary of the Temperature Effects of PNIPAAm Polymers and PNIPAAm Conjugates on 5(6)-Carboxyfluorescein-entrapped LUVs**

temperature (°C)	$\Delta f_{\text{polymer}}^a$		$\Delta f_{\text{conjugate}}^b$	
	19	20	29	30
22	0.0	0.0	12.8	0.0
35	0.0	0.0	37.9	75.0
43	12.0	41.2	48.4	87.7

<sup>a</sup>Percentage change in 5(6)-carboxyfluorescein emission at 280 s relative to LUV lysis upon the addition of polymer to the solution containing LUVs. <sup>b</sup>Percentage change in 5(6)-carboxyfluorescein emission at 280 s relative to LUV lysis upon the addition of conjugate to the solution containing LUVs.

and **30** became highly lipophilic. While stark differences in fluorescence change could be attributed to a lower initial solubility (and thus greater lipophilicity) of conjugate **29** in aqueous solutions, the fluorescence overshoot followed by a relaxation observed after the addition of conjugate **30** to the solution containing LUVs demonstrated that the turbidity of the sample overwhelmed the fluorescence emission (Figure 5b). Furthermore, addition of Triton X-100 did not lead to 100% fluorescence emission, which suggests that the 5(6)-carboxyfluorescein is interlocked as a part of the precipitate containing conjugate **30**. The role of the core cyclic peptide moiety as the central channel moiety was established through control experiments in which PNIPAAm polymers **19** and **20** caused no changes in fluorescence emission upon addition to 5(6)-carboxyfluorescein-entrapped LUVs at 20 and 35 °C (Figure S16). As Figure 5a and b demonstrates, a further increase in temperature to 43 °C followed by the addition of conjugates **29** and **30** resulted in a further increase in fluorescence emission confirming proton efflux. However, at 43 °C, incubation of the polymer precursors **19** and **20** also resulted in uncontrolled proton efflux, which suggests that in the presence of PNIPAAm precipitates the phospholipid bilayer integrity of the LUVs is perturbed (Figure S16). The disruption of the LUVs is consistent with studies of PNIPAAm bound liposomes containing doxorubicin, which suggested that the temperature-induced coil-to-globule transition of the attached PNIPAAm caused bilayer disruption.<sup>57</sup> Furthermore, despite the reversibility of the polymer LCST behavior in the absence of LUVs (Figure S15), reversing the temperature in the presence of LUVs did not result in resuspension of the precipitates obtained from mixing LUVs with conjugates **29** and **30** at high temperatures. The LCST profile of the conjugates was also confirmed through incubation with 5(6)-carboxyfluorescein-entrapped LUVs followed by heating the solution, which confirms that controlled phospholipid bilayer channel formation can be achieved using temperature as an external stimulus (Figure 5c). Despite the loss of control of well-defined phospholipid channel formation at 43 °C, temperature induced unimeric channel formation can still be achieved with conjugates ligated to PNIPAAm at an intermediate temperature of 35 °C (Figure 5d).

## CONCLUSIONS

In this contribution, the potential of cyclic peptide–polymer nanotubes is exploited as versatile, supramolecular entities that can form well-defined channels in phospholipid bilayers. The ligation of synthetic polymers to a cyclic peptide was performed via an easy and simple active-ester conjugation strategy, which permitted the modulation of the nanotube properties post-assembly without the need to design and synthesize a new cyclic peptide. By combining a conjugate library consisting of a single cyclic peptide core with polymer shells consisting of either hydrophobic or hydrophilic polymers with a series of large unilamellar vesicle assays, a structure–channel formation relationship was established. The knowledge gained from this relationship permitted the creation of a novel temperature responsive system based on poly(*N*-isopropylacrylamide) conjugates that for the first time allowed on-demand control over transbilayer channel formation. These thermoresponsive channels can provide new insights for the creation of direct transport links between the cytosol and the extracellular media. Furthermore, these direct transbilayer transport links can be envisioned as a valuable tool for devising localized, hyperthermic drug delivery that does not lead to endocytic uptake and circumvents the requirement for the drugs to undergo endosomal/lysosomal escape mechanisms to enable drug efficacy.

## ASSOCIATED CONTENT

### Supporting Information

Synthetic protocols, NMR, SEC, fluorescence, and SANS data. This material is available free of charge via the Internet at <http://pubs.acs.org>.

## AUTHOR INFORMATION

### Corresponding Authors

\*E-mail: [Kate.Jolliffe@sydney.edu.au](mailto:Kate.Jolliffe@sydney.edu.au).

\*E-mail: [S.Perrier@warwick.ac.uk](mailto:S.Perrier@warwick.ac.uk).

### Present Address

Maarten Danial, CSIRO Materials Science and Engineering, Bayview Ave., Clayton VIC 3168, Australia

### Notes

The authors declare no competing financial interest.

## ACKNOWLEDGMENTS

The Australian Research Council Discovery (K.A.J. and S. P.) and Future Fellowship (S. P.) Programmes are acknowledged for funding. Dr. Algi Serelis (Dulux, Australia) is thanked for the provision of the (propanoic acid)yl butyl trithiocarbonate chain transfer agent. Dr. Nick Proschogo is thanked for performing MALDI-FTICR and electrospray ionization–mass spectrometry on peptides and the NHS-PABTC chain transfer agent, respectively. Dr. Paul Butler and NIST are thanked for support for the SANS experiments. Dr. Paul Fitzgerald and Prof. Greg Warr are thanked for assistance with SANS experiments and help with interpreting the SANS data.

## REFERENCES

- (1) Singer, S. J.; Nicolson, G. L. *Science* **1972**, *175*, 720–731.
- (2) Matile, S.; Vargas Jentzsch, A.; Montenegro, J.; Fin, A. *Chem. Soc. Rev.* **2011**, *40*, 2453–2474.
- (3) Fyles, T. M. *Chem. Soc. Rev.* **2007**, *36*, 335–347.
- (4) Alfonso, I.; Quesada, R. *Chem. Sci.* **2013**, *4*, 3009–3019.



- (5) Montenegro, J.; Ghadiri, M. R.; Granja, J. R. *Acc. Chem. Res.* **2013**, *46*, 2955–2965.
- (6) Gong, B.; Shao, Z. *Acc. Chem. Res.* **2013**, *46*, 2856–2866.
- (7) Cazacu, A.; Tong, C.; Van Der Lee, A.; Fyles, T. M.; Barboiu, M. *J. Am. Chem. Soc.* **2006**, *128*, 9541–9548.
- (8) Otis, F.; Racine-Berthiaume, C.; Voyer, N. *J. Am. Chem. Soc.* **2011**, *133*, 6481–6483.
- (9) Madhavan, N.; Robert, E. C.; Gin, M. S. *Angew. Chem., Int. Ed.* **2005**, *44*, 7584–7587.
- (10) Badi, N.; Auvray, L.; Guégan, P. *Adv. Mater.* **2009**, *21*, 4054–4057.
- (11) McNally, B. A.; Koulov, A. V.; Lambert, T. N.; Smith, B. D.; Joos, J.-B.; Sisson, A. L.; Clare, J. P.; Sgarlata, V.; Judd, L. W.; Magro, G.; Davis, A. P. *Chem.–Eur. J.* **2008**, *14*, 9599–9606.
- (12) Helsel, A. J.; Brown, A. L.; Yamato, K.; Feng, W.; Yuan, L.; Clements, A. J.; Harding, S. V.; Szabo, G.; Shao, Z.; Gong, B. *J. Am. Chem. Soc.* **2008**, *130*, 15784–15785.
- (13) Si, W.; Chen, L.; Hu, X. B.; Tang, G.; Chen, Z.; Hou, J. L.; Li, Z. T. *Angew. Chem., Int. Ed.* **2011**, *50*, 12564–12568.
- (14) Chen, L.; Si, W.; Zhang, L.; Tang, G.; Li, Z. T.; Hou, J. L. *J. Am. Chem. Soc.* **2013**, *135*, 2152–2155.
- (15) Bröer, S. *Physiol. Rev.* **2008**, *88*, 249–286.
- (16) Ghadiri, M. R.; Granja, J. R.; Buehler, L. K. *Nature* **1994**, *369*, 301–304.
- (17) García-Fandiño, R.; Amorín, M.; Castedo, L.; Granja, J. R. *Chem. Sci.* **2012**, *3*, 3280–3285.
- (18) Clark, T. D.; Buehler, L. K.; Ghadiri, M. R. *J. Am. Chem. Soc.* **1998**, *120*, 651–656.
- (19) Sakai, N.; Matile, S. *Langmuir* **2013**, *29*, 9031–9040.
- (20) Chapman, R.; Danial, M.; Koh, M. L.; Jolliffe, K. A.; Perrier, S. *Chem. Soc. Rev.* **2012**, *41*, 6023–6041.
- (21) Sánchez-Quesada, J.; Isler, M. P.; Ghadiri, M. R. *J. Am. Chem. Soc.* **2002**, *124*, 10004–10005.
- (22) Suga, T.; Osada, S.; Kodama, H. *Bioorg. Med. Chem.* **2012**, *20*, 42–46.
- (23) Granja, J. R.; Ghadiri, M. R. *J. Am. Chem. Soc.* **1994**, *116*, 10785–10786.
- (24) Sánchez-Quesada, J.; Kim, H. S.; Ghadiri, M. R. *Angew. Chem., Int. Ed.* **2001**, *40*, 2503–2506.
- (25) Fernandez-Lopez, S.; Kim, H. S.; Choi, E. C.; Delgado, M.; Granja, J. R.; Khasanov, A.; Kraehenbuehl, K.; Long, G.; Weinberger, D. A.; Wilcoxon, K. M.; Ghadiri, M. R. *Nature* **2001**, *412*, 452–455.
- (26) Fletcher, J. T.; Finlay, J. A.; Callow, M. E.; Callow, J. A.; Ghadiri, M. R. *Chem.–Eur. J.* **2007**, *13*, 4008–4013.
- (27) Motiei, L.; Rahimpour, S.; Thayer, D. A.; Wong, C.-H.; Ghadiri, M. R. *Chem. Commun.* **2009**, 3693–3695.
- (28) Reiriz, C.; Amorín, M.; García-Fandiño, R.; Castedo, L.; Granja, J. R. *Org. Biomol. Chem.* **2009**, *7*, 4358–4361.
- (29) Ghadiri, M. R.; Granja, J. R.; Milligan, R. A.; McRee, D. E.; Khazanovich, N. *Nature* **1993**, *366*, 324–327.
- (30) De Santis, P.; Morosetti, S.; Rizzo, R. *Macromolecules* **1974**, *7*, 52–58.
- (31) Chapman, R.; Jolliffe, K. A.; Perrier, S. *Aust. J. Chem.* **2010**, *63*, 1169–1172.
- (32) Chapman, R.; Jolliffe, K. A.; Perrier, S. *Polym. Chem.* **2011**, *2*, 1956–1963.
- (33) Couet, J.; Jeyaprakash, J. D.; Samuel, S.; Kopyshv, A.; Santer, S.; Biesalski, M. *Angew. Chem., Int. Ed.* **2005**, *44*, 3297–3301.
- (34) Couet, J.; Biesalski, M. *Macromolecules* **2006**, *39*, 7258–7268.
- (35) ten Cate, M. G. J.; Severin, N.; Börner, H. G. *Macromolecules* **2006**, *39*, 7831–7838.
- (36) Chiefari, J.; Chong, Y. K.; Ercole, F.; Krstina, J.; Jeffery, J.; Le, T. P. T.; Mayadunne, R. T. A.; Meijs, G. F.; Moad, C. L.; Moad, G.; Rizzardo, E.; Thang, S. H. *Macromolecules* **1998**, *31*, 5559–5562.
- (37) Moad, G.; Rizzardo, E.; Thang, S. H. *Aust. J. Chem.* **2012**, *65*, 985–1076.
- (38) Perrier, S.; Takolpuckdee, P. *J. Polym. Sci., Part A: Polym. Chem.* **2005**, *43*, 5347–5393.
- (39) Danial, M.; Tran, C. M.-N.; Young, P. G.; Perrier, S.; Jolliffe, K. A. *Nat. Commun.* **2013**, *4*, 2780.
- (40) Matile, S.; Sakai, N.; Hennig, A. Transport Experiments in Membranes. In *Supramolecular Chemistry: From Molecules to Nanomaterials*; Gale, P. A., Steed, J. W., Eds.; John Wiley & Sons, Ltd: Hoboken, NJ, 2012; pp 473–499.
- (41) Thomas, J. A.; Buchsbaum, R. N.; Zimniak, A.; Racker, E. *Biochemistry* **1979**, *18*, 2210–2218.
- (42) Carmichael, V. E.; Dutton, P. J.; Fyles, T. M.; James, T. D.; Swan, J. A.; Zojaji, M. *J. Am. Chem. Soc.* **1989**, *111*, 767–769.
- (43) Cheng, T.; Zhao, Y.; Li, X.; Lin, F.; Xu, Y.; Zhang, X.; Li, Y.; Wang, R.; Lai, L. *J. Chem. Inf. Model.* **2007**, *47*, 2140–2148.
- (44) Tetko, I. V.; Gasteiger, J.; Todeschini, R.; Mauri, A.; Livingstone, D.; Ertl, P.; Palyulin, V. A.; Radchenko, E. V.; Zefirov, N. S.; Makarenko, A. S.; Tanchuk, V. Y.; Prokopenko, V. V. *Comput.-Aided Mol. Des.* **2005**, *19*, 453–463.
- (45) Davis, J. T.; Gale, P. A.; Okunola, O. A.; Prados, P.; Iglesias-Sánchez, J. C.; Torroba, T.; Quesada, R. *Nat. Chem.* **2009**, *1*, 138–144.
- (46) Gabriel, G. J.; Pool, J. G.; Som, A.; Dabkowski, J. M.; Coughlin, E. B.; Muthukumar, M.; Tew, G. N. *Langmuir* **2008**, *24*, 12489–12495.
- (47) Chapman, R.; Warr, G. G.; Perrier, S.; Jolliffe, K. A. *Chem.–Eur. J.* **2013**, *19*, 1955–1961.
- (48) Chapman, R.; Koh, M. L.; Warr, G. G.; Jolliffe, K. A.; Perrier, S. *Chem. Sci.* **2013**, *4*, 2581–2589.
- (49) Neumann, E.; Schaefer-Ridder, M.; Wang, Y.; Hofschneider, P. H. *EMBO J.* **1982**, *1*, 841–845.
- (50) Ferrara, K.; Pollard, R.; Borden, M. *Annu. Rev. Biomed. Eng.* **2007**, *9*, 415–447.
- (51) Plank, C.; Zelphati, O.; Mykhaylyk, O. *Adv. Drug Delivery Rev.* **2011**, *63*, 1300–1331.
- (52) Petros, R. A.; DeSimone, J. M. *Nat. Rev. Drug Discovery* **2010**, *9*, 615–627.
- (53) Singhal, R.; Orynbayeva, Z.; Sundaram, R. V. K.; Niu, J. J.; Bhattacharyya, S.; Vitol, E. A.; Schrlau, M. G.; Papazoglou, E. S.; Friedman, G.; Gogotsi, Y. *Nat. Nanotechnol.* **2011**, *6*, 57–64.
- (54) Chen, W.-H.; Regen, S. L. *J. Am. Chem. Soc.* **2005**, *127*, 6538–6539.
- (55) Chilkoti, A.; Dreher, M. R.; Meyer, D. E.; Raucher, D. *Adv. Drug Delivery Rev.* **2002**, *54*, 613–630.
- (56) Chapman, R.; Bouten, P. J. M.; Hoogenboom, R.; Jolliffe, K. A.; Perrier, S. *Chem. Commun.* **2013**, *49*, 6522–6524.
- (57) Ta, T.; Convertine, A. J.; Reyes, C. R.; Stayton, P. S.; Porter, T. M. *Biomacromolecules* **2010**, *11*, 1915–1920.